Applied Clay Science 219 (2022) 106444

Contents lists available at ScienceDirect

Applied Clay Science

journal homepage: www.elsevier.com/locate/clay

Kaolin group minerals under pressure: The study of their structural and electronic properties by DFT methods

D. Richard [a,b,*], N.M. Rendtorff [a,b]

[a] CETMIC, Centro de Tecnología de Recursos Minerales y Cerámica (CONICET La Plata - CIC PBA - UNLP). Camino Centenario y 506, CC 49, (B1897ZCA), M. B. Gonnet, Buenos Aires, Argentina
[b] Facultad de Ciencias Exactas, Universidad Nacional de La Plata, 47 y 115, La Plata, Buenos Aires, Argentina

ARTICLE INFO

Keywords:
Kaolin group minerals
DFT
Bulk modulus
Transformation pressure
DOS
Bandgap

ABSTRACT

Kaolinites have a wide impact in many technological applications, and also are promising for their potential new uses in the future. Because these clay minerals naturally exist as fine particles, there are difficulties in making measurements of their bulk structural and electronic properties. Also, the occurrence of stacking faults and the presence of structural defects at the nanoscale, make these clay minerals quite complex systems to propose accurate models at the crystallographic scale.

This work presents a study of six different kaolin group polytypes using calculations based on the Density Functional Theory (DFT), and includes the naturally occurring clay minerals kaolinite, dickite, and nacrite, and also other three pressure-induced polytypes that have been experimentally observed. The idealized structures were optimized using DFT methods, and their responses to hydrostatic pressure were theoretically analyzed from energy *vs.* volume and enthalpy *vs.* pressure data. From these, the bulk modulus for each polytype was predicted, and their relative stability and the potential transformations between structures were discussed. Finally, the electronic density of states for each polytype was calculated and compared to each other.

The results indicate that although structurally these polytypes present significant differences between each other that lead to different elastic responses, from the perspective of the electronic properties they may be indistinguishable. The analysis performed in this work can be helpful as guidance and for interpretation in future experiments.

1. Introduction

Clay minerals are phyllosilicates found in most of the sedimentary rocks in the Earth's upper crust. Since then, the study of their structural and elastic properties is of great importance for researchers in geochemistry, geophysics, seismology, and high-pressure mineral physics (Wang et al., 2001; Vanorio et al., 2003; Fossum, 2012; Balan et al., 2014; Seredin et al., 2018; Soto et al., 2021; Zhang et al., 2021). Among the clay minerals, kaolin is the largest mined clay, and is commonly used in ceramics, cement, refractories, and as paper coating and filling. Kaolins have a wide impact in many current scientific and technological applications, and also have a great potential for use in the future (Schroeder and Erickson, 2014; Detellier, 2018; Yang et al., 2020; Zhao et al., 2021). From the experimental point of view, there are difficulties in making direct measurements of the structural and elastic properties of these clay minerals. This is mainly because such properties are commonly measured on single crystals, but kaolins naturally exist as fine particles with variable compositions, and clay crystals large enough for direct measurements are extremely hard to find in nature (Bayuk et al., 2007). As a consequence, a wide range of experimental values can be found in the literature for the same measured quantity. For example, in the case of kaolinite, which is the main clay mineral in the kaolin group, elastic bulk moduli from 1.4 to about 60 GPa have been reported (Wang et al., 2001; Mikowski et al., 2007; Benazzouz and Zaoui, 2012a; Weck et al., 2015; Hwang et al., 2017). On the other hand, different strategies have emerged to compare raw kaolins to idealized structural models according to the degree of structural order or 'crystallinity' they contain (Andrini et al., 2016; Sakharov et al., 2016; Richard et al., 2022). In addition, among other structural features, polytypism is common in clay minerals, when layers of identical structure and

* Corresponding author at: CETMIC, Centro de Tecnología de Recursos Minerales y Cerámica (CONICET La Plata - CIC PBA - UNLP). Camino Centenario y 506, CC 49, (B1897ZCA), M. B. Gonnet, Buenos Aires, Argentina.
E-mail address: richard@fisica.unlp.edu.ar (D. Richard).

https://doi.org/10.1016/j.clay.2022.106444
Received 5 November 2021; Received in revised form 3 February 2022; Accepted 4 February 2022
Available online 11 February 2022

composition are arranged with a different stacking scheme (Brigatti et al., 2006). In the case of the kaolin group, kaolinite is complemented by other two naturally occurring layer structures with the same general composition but different stacking sequence: the dickite and nacrite polytypes. Kaolinite is very abundant on Earth's surface, and dickite is also very common, whereas nacrite is more uncommon (Murray, 1988; Brigatti et al., 2006). During the last decades, it has been analyzed and discussed the existence of additional polytypes into this group, considering other possible stacking sequences (Newnham, 1961; Dera et al., 2003; Kogure and Inoue, 2005; Kogure et al., 2010; Welch and Crichton, 2010; Welch et al., 2012; Balan et al., 2014; Teixeira et al., 2017). More recently, Mercier and Le Page (2008, 2009, 2011) studied the stability of many theoretical polytype models using *ab initio* calculations based on the Density Functional Theory (DFT). In their works, more than 50 geometrically distinguishable stacking modes for kaolinite sheets were assessed, concluding that known polytypes (kaolinite, dickite, and nacrite) are stable at 0 K and ambient pressure, but there are other polytypes energetically competitive, which might crystallize at ambient pressure. Currently, according to the experiments, it is known that polytype transformations can occur in kaolinite and dickite by applying relatively low pressures (Johnston et al., 2002; Dera et al., 2003; Welch and Crichton, 2010; Welch et al., 2012; Hwang et al., 2017). Using synchrotron X-ray powder diffraction, Welch and Crichton (2010) found that kaolinite K-I (the most familiar polytype) transforms to phases K-II and K-III at ~3.7 and ~7 GPa, respectively. In that work, the diffraction patterns were successfully related with those corresponding to the structural models previously predicted with *ab initio* methods by Mercier and Le Page (2008, 2009, 2011), Mercier et al. (2010). On the other hand, Dera et al. (2003) used single-crystal X-ray diffraction and diamond-anvil cell techniques and found that, above 2 GPa, dickite transforms to a high-pressure phase (HP-dickite). Although these experiments gave actual evidence of other possible polytypes in addition to the naturally occurring ones, the experimental conditions make difficult the measurement of additional properties in those polytypes, such as the bulk moduli or electric properties.

This work presents a DFT study of the response to the hydrostatic pressure of the six experimentally observed kaolin group polytypes. With this methodology, the relative stability of such polytypes under pressure is studied, and the equilibrium structures and bulk moduli are determined. In addition, the density of electronic states is analyzed in each case. The DFT predictions allow a better understanding of the structural, elastic, and electronic properties in these kaolin group polytypes, and provide theoretical guidance for other areas in which clay mineral modeling involves such properties, as well as for technological applications in which clay processing may produce polytype transformations.

2. Materials and methods

Clay minerals in the kaolin group are 1:1 dioctahedral sheet silicates with general composition $Al_2Si_2O_5(OH)_4$, being kaolinite, dickite, and nacrite their naturally occurring polytypes (Brigatti et al., 2006). In this work, DFT calculations were used to study these polytypes, together with three additional polytypic forms for kaolinite and dickite that have been observed when pressure is applied (Dera et al., 2003; Welch and Crichton, 2010). The starting structures correspond to those available in the literature: the K-I structure (Kaol, the familiar kaolinite polytype) was taken from Richard and Rendtorff (2019), and the K-II and K-III phases were taken from the works of Mercier and Le Page (2008, 2009) (where are called K5a and model 18, respectively). On the other hand, the starting structures for dickites (dickite and HP-dickite) were taken from the work of Dera et al. (2003). Finally, the nacrite structure is that reported by Zhukhlistov (2008). Polytypes K-I, K-II, and K-III are single-layer models, while dickite and nacrite present a two-layer stacking sequence. All these starting structures are represented in Fig. 1. As can be seen, the architecture of these clay composite layers are the same, and

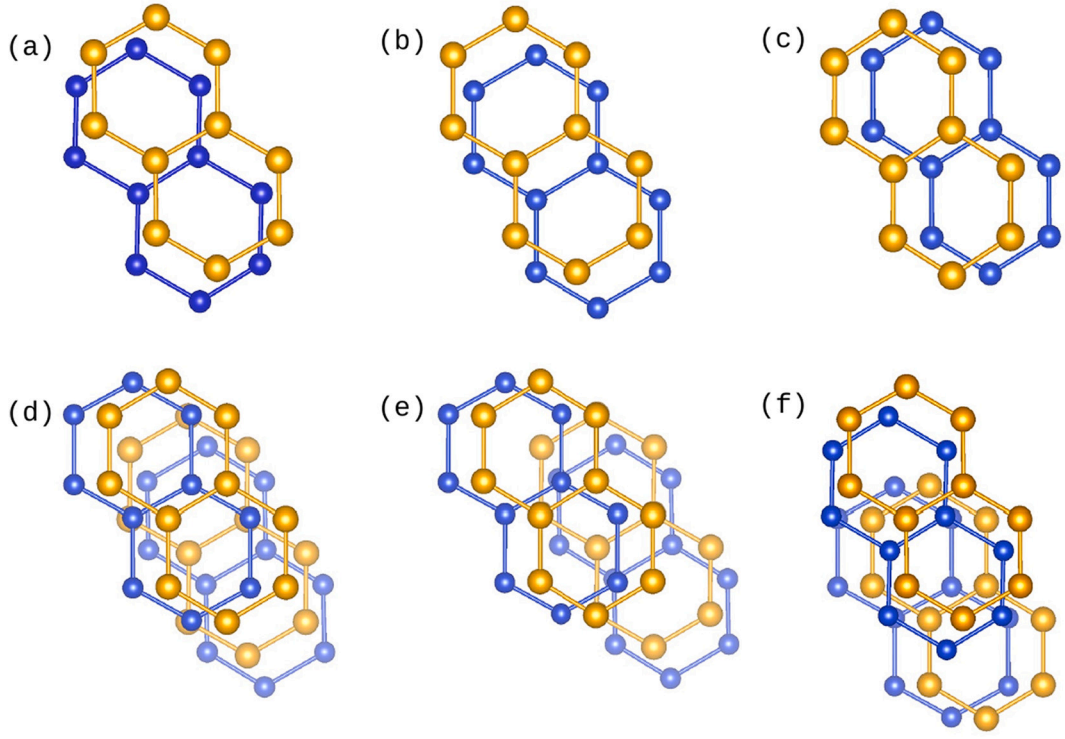

Fig. 1. Overlapping of neighboring layers in the studied kaolin group polytypes: (a) Kaol K-I, (b) K-II, (c) K-III, (d) dickite, (e) HP-dickite, and (f) nacrite. Orange spheres stand for Al atoms, and blue spheres for Si atoms. All projections are shown normal to the layers, with the O and H atoms omitted for better visualization. For the two-layer stacking sequence in (d-f), the atoms in lighter colors correspond to those of the lower layer. (For interpretation of the references to color in this figure legend, the reader is referred to the web version of this article.)

only differ in the way the Si and Al sheets are stacked over one another, which lead to different sequences for the position of octahedral vacancies in the adjacent layers. Compared to K-I (Fig. 1a), the K-II (Fig. 1b) and K-III (Fig. 1c) polytypes involve a shift of the Si and Al sheets with respect to each other, being K-III also characterized by a more important contraction in the *a-b* plane. On the other hand, compared to dickite (Fig. 1d), the HP-dickite (Fig. 1e) structure involves a displacive mechanism in the two-stacking sequence, the topology of the individual 1:1 layers in both dickites remains practically unchanged after the transformation, but their stacking scheme is different, as reflected in the change of the superimposed Al and Si atoms of the different layers from one polytype to another. Finally, in addition to its stacking sequence, nacrite (Fig. 1f) is characterized by its smaller lateral dimensions and greater interlayer separation than dickite and kaolinite.

The calculations were performed with the open-source Quantum ESPRESSO (QE) package, which is based on pseudopotentials and plane waves (Giannozzi et al., 2017). Two generalized-gradient approximations for the exchange and correlation energy were considered: the long-time standard parameterized by Perdew et al. (1996) (PBE), and the more accurate approximation for solids parameterized by Wu and Cohen (2006) (WC). In addition, the semiempirical D2 version of Grimme's dispersion was used to assess the effect of London long-range electron correlations (Grimme, 2006). These elections were made after considering the performance of the PBE and WC semilocal functionals (Tran et al., 2007; Haas et al., 2009) and the importance of the long-range dispersive corrections for the description of clay minerals (Tunega et al., 2012). The PBE and WC projector augmented-wave pseudopotentials were taken from the high-accuracy library generated by Dal Corso (2014) (Prandini et al., 2018), using the following valence states: Si(3s, 3p), Al(3s, 3p), O(2s, 2p), and H(1s). DFT results were obtained after checking the energy convergence of the calculations. A kinetic energy cutoff of 100 Ry was used, and the *k*-space Monkhorst-Pack grid was of 6x6x6 and 6x6x3 for single layer, and two-layer structures, respectively. The optimized structures were determined by minimizing the total energy with variable cell calculations, and allowing the atoms to relax until the forces on them were 0.025 eV/Å or less. This methodology is the same as that successfully used in other recent studies for the Kaol structure (Richard and Rendtorff, 2019, 2021). For each system, the obtained optimized structure was the starting point to calculate energy *vs.* volume ($E(V)$) data under hydrostatic deformation: the unit cell was deformed hydrostatically and then the energy was recalculated for at least 10 different values of V (the variations in V were within 10% of the equilibrium value). For each volume, the internal atoms were allowed to relax again using the same force criteria as above. The Birch-Murnaghan equation of state (EOS) was fitted to $E(V)$ to determine the zero-pressure bulk modulus (B_0) (Birch, 1947; Pavese, 2005), and the polytype stability as a function of pressure was studied through the comparison of the enthalpy $H(P) = E + PV$ between polytypes, from which the transition pressures can be evaluated (Mercier and Le Page, 2008; Richard et al., 2016). Also, X-ray diffraction patterns for each polytype were simulated using the VESTA software (Momma and Izumi, 2011). Finally, the electronic properties were analyzed by calculating the density of electronic states (DOS) for each polytype at different pressures.

3. Results

3.1. Polytype structures and stability

The optimized cell parameters of the considered polytypes together with reference experimental data are given in Table 1. For each unit cell, the lattice parameters are provided using the same space group as that of the corresponding experimental entry (primitive space group *P1* for K-I, K-II, and K-III, and monoclinic space group *Cc* for dickite, HP-dickite, and nacrite). All the atomic positions of the optimized structures are provided as supplementary material. For an easier global comparison

Table 1
Comparison between PBE, WC, and experimental data of the unit cell parameters of kaolin group polytypes and their bulk moduli. Experimental values were taken from [a] Welch and Crichton (2010), [b] Hwang et al. (2017), [c] Bish (1993), [d] Dera et al. (2003), [e] Zhukhlistov (2008), and [f] Hwang et al. (2020). *Value that comes from extrapolation to zero pressure.

Polytype	a (Å)	b (Å)	c (Å)	α (°)	β (°)	γ (°)	V per formula unit (Å^3)	E_0 per formula unit (eV)	B_0 (GPa)
K-I									
PBE	5.185	8.998	7.347	91.76	105.10	89.84	165.410	−7522.543	71.3(3)
WC	5.139	8.920	7.230	91.53	105.12	89.78	159.918	−7468.720	77.9(3)
Experimental[a]	5.1542(4)	8.9307(5)	7.3936(6)	91.879(8)	104.550(8)	89.783(9)	164.62(2)		59.7(7)
Experimental[b]	5.1555(5)	8.938(1)	7.3949(5)	91.682(8)	104.651(9)	89.804(9)	164.77(2)		58.8(4)-60.7(4)
Experimental[c]	5.1535(3)	8.9419(5)	7.3906(4)	91.926(2)	105.046(2)	89.797(2)	164.35(3)		
K-II									
PBE	5.211	5.190	7.582	89.37	72.44	119.96	166.073	−7522.486	60(2)
WC	5.150	5.132	7.434	89.59	72.12	119.92	158.996	−7468.653	58(1)
Experimental[a]							~160*		
Experimental[b]							~165*		53.7(6)-57(1)
K-III									
PBE	5.162	5.177	7.782	104.44	98.29	119.88	165.438	−7522.512	55.4(4)
WC	5.077	5.096	7.665	105.38	97.23	119.75	157.957	−7468.685	58.4(7)
Experimental[a]	5.0780(4)	5.0932(6)	7.0467(9)	97.65(1)	95.81(1)	119.95(1)	154.7(3)		55.9(1.9)
Dickite									
PBE	5.159	8.934	14.410	90	96.310	90	165.043	−7522.567	62.6(4)
WC	5.097	8.816	14.204	90	96.160	90	158.651	−7468.751	64.6(3)
Experimental[d]	5.161(3)	8.960(6)	14.459(10)	90	96.77(1)	90	165.99(5)		88.8
HP-Dickite									
PBE	5.185	8.940	14.188	90	89.08	90	164.398	−7522.542	58(1)
WC	5.123	8.825	13.894	90	88.98	90	157.017	−7468.725	62(1)
Experimental[d]							~158.5*		107.6
Nacrite									
PBE	8.903	5.163	14.519	90	99.35	90	164.633	−7522.572	59.8(2)
WC	8.794	5.106	14.279	90	99.21	90	158.230	−7468.759	62.5(1)
Experimental[e]	8.910(3)	5.144(2)	14.593(3)	90	100.50(3)	90	164.411		
Experimental[f]	8.916(1)	5.152(1)	14.612(1)	90	100.41(3)	90	165.03(2)		46.9(7)

between polytypes, in Table 1 the volume V per formula unit is also given. In the case of K-II and HP-dickite, which are polytypes that have not been observed at ambient conditions, the experimental V is an estimate that comes from extrapolation to zero pressure. On the other hand, K-III cell parameters are those measured at ambient conditions after kaolinite decompression (Welch and Crichton, 2010). Table 1 also includes the energy E_0 per formula unit corresponding to each optimized structure. First, the case of Kaol K-I can be analyzed, which is the most documented polytype among those in the table. As can be seen, PBE and WC predict lattice parameters with differences up to about 0.12 Å in the case of c, which represent a difference of 1.5%. These differences between both approximations are significantly larger than those observed between experiments (see Table 1, where several different measurements are included to illustrate the uncertainty in experimental data). The deviation obtained with WC represents a significant error in the prediction of the experimental K-I structure, and is due to a poor description of the lattice vector c, along which the hydrogen bonds between layers are formed. This comparison between PBE and WC performances when used to predict the same quantity contribute to assessing the accuracy of DFT. As can be seen in Table 1, PBE provides the best results, with an overestimation of K-I experimental volume V below 0.7%, while WC underestimates it by ~3%. In the literature, PBE is also preferred for the prediction of the K-I structure due to its good performance compared to other functionals (Sato et al., 2004; Tunega et al., 2012; Weck et al., 2015; Zhao et al., 2020; Shafei et al., 2021). Considering all these factors, the PBE results will be analyzed in what follows. In a general view to these functional predictions presented in Table 1, it is observed that for each polytype PBE overestimates the experimental V, being the only exception in the case of dickite (where it predicts V about 2% below the experimental value). When the pressure-induced polytypes are compared to those of ambient pressure it is observed that PBE predicts that for the K-I/K-II/K-III series the three polytypes have very similar volumes (there is a slight increment on V in this series of about 0.4%), and that HP-dickite has lower V than dickite. A more detailed analysis of the relative stability under pressure will be discussed later.

In Fig. 2 the $E(V)$ curves for hydrostatic deformation are presented. The V and E_0 values at the curve minima correspond to the optimized structures already included in Table 1, and the differences between minimum energies indicate the relative stability among polytypes. As can be seen, starting from those polytypes with lower E_0 energies at the curve minima, PBE indicates that nacrite, dickite, and Kaol K-I are the most stable ones. Many experimental studies (De Ligny and Navrotsky, 1999; Fialips et al., 2003; Manning, 2003; Kiseleva et al., 2011; Cuadros et al., 2014), and also some theoretical studies (Sato et al., 2004; Mercier and Le Page, 2008, 2011) have discussed what polytype has the lowest energy, but a general conclusion still remains elusive. According to the results of Fig. 2, the present calculations show that nacrite is energetically preferred, but the energy differences between the $E(V)$ minima are quite small: from nacrite to K-I are less than 50 meV (~5 kJ/mol), which corresponds to thermal activation energies below 600 K. Nevertheless it must be mentioned that, after crystallization, transformations between K-I, dickite and nacrite are not possible because they would involve rotations of contiguous layers with respect to one another. On the contrary, transitions to the corresponding higher-pressure polytypes involve a shift between adjacent sheets with no rotation. So, such transitions can happen because do not mean long-range transformations (see Fig. 1).

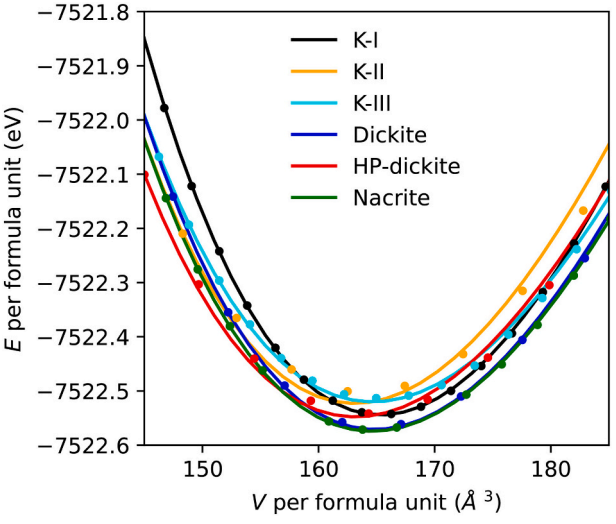

Fig. 2. $E(V)$ data for kaolin group polytypes calculated with PBE. The solid lines are the Birch-Murnaghan EOS fits.

The solid lines in Fig. 2 stand for the Birch-Murnaghan EOS fit to each $E(V)$ curve, from which the corresponding bulk modulus B_0 at zero pressure was determined. B_0 expresses the clay mineral resistance to volume change with strain-stress and serves as indicative of its resistance to fracture. During the EOS fitting procedure, the bulk modulus pressure derivative B_0' was kept fixed in 4 for easier comparison between polytypes. The obtained values for B_0 are those included in Table 1, last column. The obtained predictions denote that high-pressure polytypes have lower values of B_0 than low-pressure ones. In the case of kaolinite, B_0 values decrease from above 70 GPa in K-I, to about 55 GPa in K-III, which means a decrease of ~25%. In a similar way, in HP-dickite the B_0 value is ~15% lower than that obtained in dickite. When these DFT predictions for B_0 are compared to the experimental values, many differences arise. Although for kaolins a wide range of experimental values of B_0 has been reported, Table 1 includes those B_0 values that have been experimentally determined for the polytypes considered in this work (Dera et al., 2003; Welch and Crichton, 2010; Hwang et al., 2017). As commented above, making direct measurements of B_0 is a challenging task. Therefore, some definitive results are still pending. In the work of Welch and Crichton (2010), for K-II the available experimental data was too few and restricted to a small pressure range (3.9 to 6.5 GPa) to allow an estimate of B_0. More recently, Hwang et al. (2017) revisited the transitions observed by Welch and Crichton (2010) and determined B_0 values in the range 53.7(6)-57(1) GPa for K-II. On the other hand, the B_0 values in dickite are those of Dera et al. (2003), which were determined based only on two data points. In addition to these experimental difficulties in the measurement of B_0, it must be mentioned that the present DFT predictions are performed at 0 K on idealized defect-free structures, so differences between calculations and measurements should be expected. Nevertheless, the predicted values for B_0 of Table 1 are in good agreement with available DFT data in the literature. For example, for Kaol K-I, using *ab initio* calculations it has been reported B_0 values in the range 23–77.8 GPa (Sato et al., 2005; Benazzouz and Zaoui, 2012a; Weck et al., 2015; Zhao et al., 2020; Shafei et al., 2021). In regard to the B_0 dependence with temperature, a previous theoretical investigation in Kaol K-I indicates that, from 0 K to room temperature, B_0 decreases with temperature about 25% (Weck et al., 2015). So, the DFT values for B_0 presented in Table 1 are valid and can assist from a nanoscopic viewpoint in determining bulk moduli experimentally. In particular, if is considered that kaolin group polytypes other than K-I have been less studied in the literature. Later in this work, it will be discussed the dependence of the bulk modulus on pressure.

Fig. 3 compares relative stability considering enthalpy differences $\Delta H(P)$ between a given polytype and Kaol K-I. These curves were determined from polynomial fits to $H(P)$ data obtained with PBE and considering the conversion 1 eV per Kaol formula unit = 96 kJ/mol (a detailed description about the fitting procedure is included in the supplementary material). The range of ΔH values that Fig. 3 covers is in the order of the free-energy measurements on natural samples reported in different experimental studies (De Ligny and Navrotsky, 1999; Fialips et al., 2003; Kiseleva et al., 2011). According to the results of Fig. 3, at zero pressure, ΔH allows visualizing the most stable polytypes, as

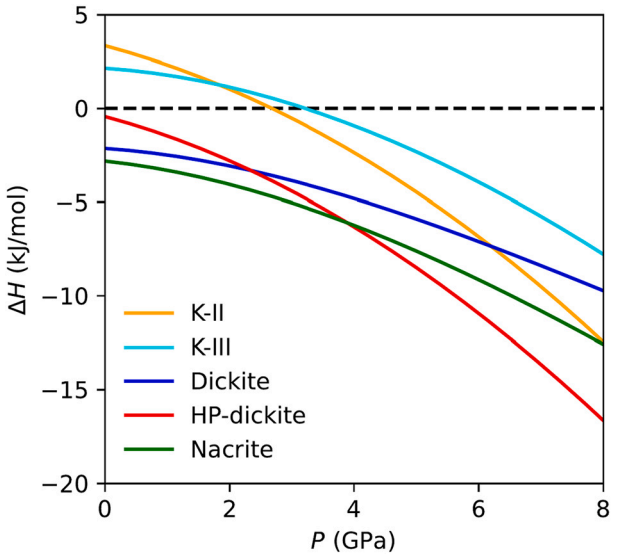

Fig. 3. Enthalpy differences ΔH with respect to Kaol K-I polytype as a function of hydrostatic pressure obtained with PBE.

commented above when $E(V)$ curves were presented. As can be seen, when no pressure is applied, the calculations indicate that Kaol K-I is more stable than K-II and K-III, and dickite and nacrite have lower enthalpies than K-I (about 4 kJ/mol below). When pressure is applied, K-I and dickite transforms into their higher-pressure polytypes through first-order transitions. The case of dickite to HP-dickite is easier to interpret, because according to PBE HP-dickite becomes the stable polytype when pressure is about 2.2 GPa. This result is in good agreement with the experimental observations of Dera et al. (2003), which indicate above 2 GPa dickite transforms to HP-dickite. On the other hand, results in Fig. 3 also indicate that at ~3 GPa K-II becomes more stable than K-I, but K-III has enthalpies so competitive that it might crystallize also at ~3 GPa. The enthalpy difference of K-III with K-II increases with pressure, making K-II the stable polytype for PBE.

In Fig. 4a are presented the predicted polytype transformations with PBE using the *P-V* data, as an alternative approach to present the results. In each plot, the solid line represents the stable structure at a given pressure, and the dotted vertical lines (for kaolinite and dickite) indicate the transformation between polytypes. As can be seen, both K-I/K-II and dickite/HP-Dickite transformations involve a volume contraction below 3%. On the other hand, in order to show how the structure of each polytype changes internally when pressure is applied, Fig. 4b presents the distance between contiguous layers as a function of pressure. This distance is measured between 001 planes passing through Si and Al atoms after structural relaxation, and it must serve as a reference of the interlayer distance (Guggenheim et al., 2009). Fig. 4b indicates that at $P = 0$ GPa all polytypes present a similar interlayer distance (in the range 4.3–4.4 Å), with the exception of K-III, where this distance is about 10% higher than the rest. Although this polytype is more compact than K-I and K-II, as indicated by its unit cell volume *V*, the greater value of its interlayer distance (and its lattice parameter *c*) is compensated by a contraction over the *a-b* plane (see Table 1). On the other hand, according to Fig. 4b, when pressure is applied the interlayer distance slightly decreases, reaching at $P = 8$ GPa a value about 5% lower than the starting one.

Fig. 5 presents the bulk modulus as a function of pressure, and comes from the polynomial fits to $V(P)$ data of Fig. 4a, using the formula $B = -V/(\partial V/\partial P)$. In general, the bulk modulus increases with pressure in all polytypes, and at 8 GPa it is about 50% higher than its zero-pressure value. These results are in good agreement with the molecular dynamics calculations for the K-I polytype presented in the works of Benazzouz and Zaoui (2012a, 2012b).

In the supplementary material are included data for $E(V)$, $\Delta H(P)$, *V*

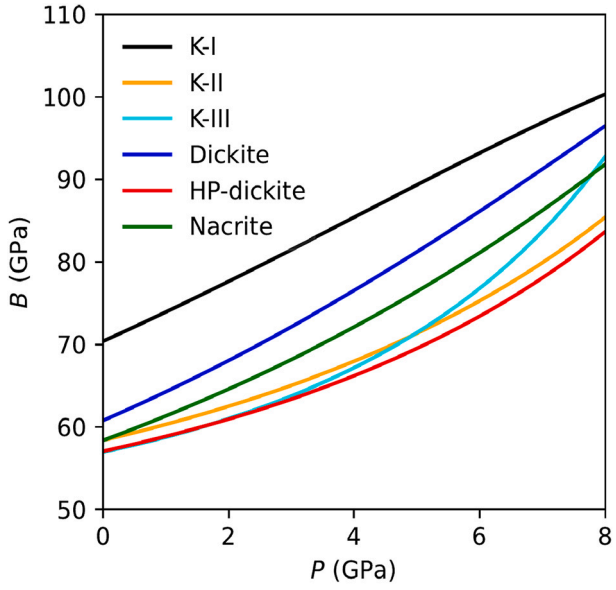

Fig. 5. Variation of bulk modulus as function of pressure between 0 and 8 GPa obtained with PBE.

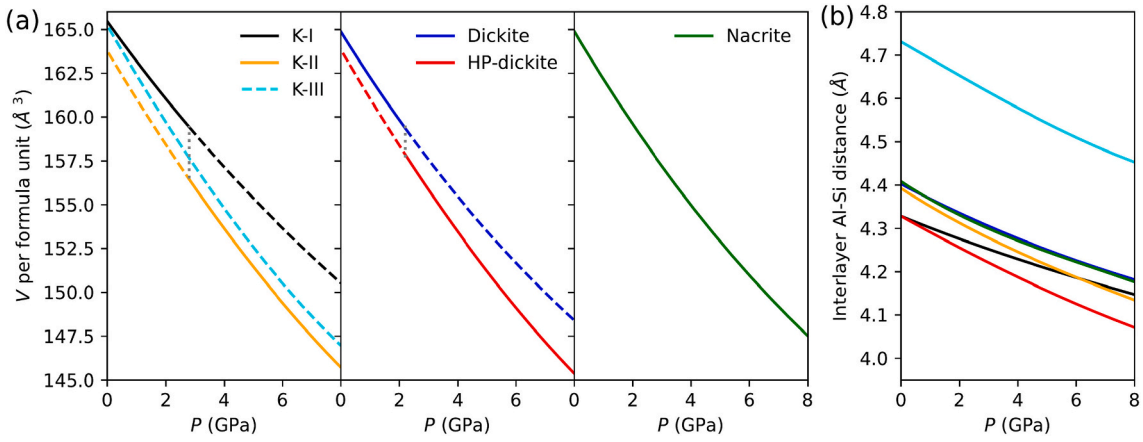

Fig. 4. PBE results for (a) volume as a function of pressure in kaolinite (left), dickite (center), and nacrite (right) polytypes, and (b) interlayer distance as a function of pressure (using same color codes as in fig. (a)). In (a), solid lines indicate the predicted stable structures according to ΔH data.

(P), and $B(P)$ obtained with WC, and compared to PBE (see Figs. S1-S4). When pressure is applied, both PBE and WC provide similar $\Delta H(P)$ results, with a major difference in the case of K-II: WC indicates that at ~2 GPa is the K-III polytype the one that becomes more stable than K-I, while K-II is less stable. As mentioned above, the experimental observations indicate that K-I transforms to K-II and K-III at ~3.7 and ~7 GPa, respectively (Welch and Crichton, 2010; Hwang et al., 2017), but according to the differences between PBE and WC predictions (Figs. S2 and S3), there is no unambiguous conclusion from DFT calculations about what polytype, K-II or K-III, becomes more stable when pressure is applied to K-I. Nevertheless, they clearly indicate that above 2 GPa transformations to these other polytypes are more possible. The bias between the different DFT predicted transition pressures is attributed to the limited accuracy of the calculation methods when used for this purpose. Also, another difference between PBE and WC can be observed in the $B(P)$ curves (Fig. S4). Although at zero-pressure both approximations give the B_0 values presented in Table 1, compared to PBE, WC predicts more significant changes in the $B(P)$ curve slope as pressure increases. This behavior is attributed to a limit of validity of the polynomial fits used to compute the derivatives needed for $B(P)$.

As an additional aid to follow the structural differences between K-I, K-II, and K-III during transformation, in Fig. 6 are presented the theoretical X-ray diffraction patterns for the optimized structures. These patterns correspond to $\lambda = 0.6199$ Å, which is the wavelength used in the synchrotron experiments of Hwang et al. (2017). As can be seen, the transition from K-I to K-II produces a very significant change in the diffraction pattern near $2\vartheta = 15°$, where new reflections arise. These peaks later disappear with the transition from K-II to K-III, as also has been experimentally observed (Hwang et al., 2017). A similar analysis can be done for the dickite to HP-dickite transition. In the supplementary material are provided diffraction patterns for the other polytypes for further comparisons, and also those predicted with WC are included (see Fig. S5).

As a final remark of this section, the obtained polytype structures and relative stability through DFT calculations follow the experimental observations. Also, a similar DFT description for $\Delta H(P)$ has been roughly done in the work of Mercier and Le Page (2008). As commented earlier, the transitions from K-I to K-II/K-III and from dickite to HP-dickite only involve shifts between adjacent sheets, with no rotation between contiguous layers (see Fig. 1), so they can happen during the high-pressure experiments. So, the present calculations may help in the study of the relative stability of these polytypes, which includes some structures that are difficult to access experimentally. But also the structures of high pressures may provide insights into the nature of the stacking disorder in raw kaolins. Therefore, at this point, the DFT calculations presented in the current work can provide an additional reference for defining criteria in future experiments where the structural properties and compressional behavior of kaolins are studied.

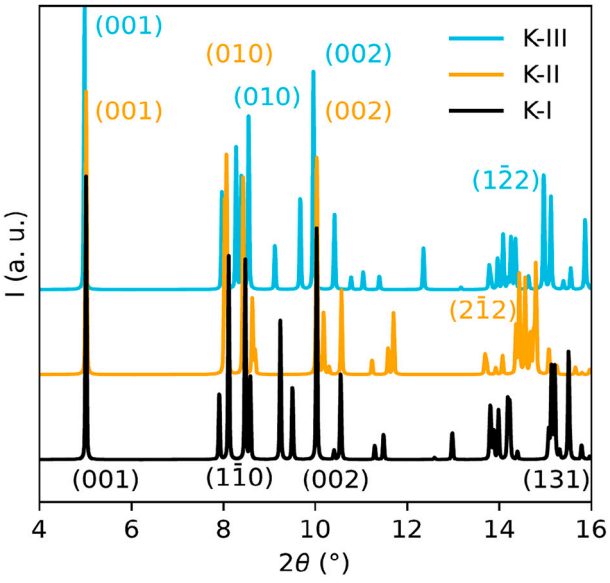

Fig. 6. X-ray diffraction patterns for K-I, K-II, and K-III polytypes with PBE and $\lambda = 0.6199$ Å. The Miller indices of most prominent peaks in each region are indicated following the color codes.

3.2. Density of electronic states

Once the optimized structures for each polytype were found, their DOS were calculated. In Fig. 7a are presented the DOS obtained with the PBE approximation, where zero energy is at the Fermi level (E_F). The DOS in solid lines correspond to the $P = 0$ GPa situation, and those in dotted lines to $P = 8$ GPa. As can be seen, all considered polytypes are insulators with very similar DOS to each other: a valence band (VB) of about 10 eV width is separated from a conduction band (CB) by an energy bandgap (E_g) slightly above 5 eV. In Table 2 are presented the numerical values for E_g in each case, and indicate that the more compact polytypes have slightly larger bandgap energies. The results with the WC approximation follow the same general trend (see supplementary material, Fig. S6 and Table S2). In addition, all the DOS of Fig. 7a are in very good agreement with those previously reported using first-principles methods in Kaol K-I (Nisar et al., 2011; Fang et al., 2017; Richard and Rendtorff, 2019; Zhao et al., 2020; Shafei et al., 2021), being known that standard DFT methods underestimate the experimental value of E_g (Mori-Sánchez et al., 2008). Nevertheless, these calculation results can be used to compare the fine structure of the DOS of the different kaolin group polytypes, which is an analysis not found in the literature. The similarities between the zero-pressure DOS of Fig. 7a (in solid lines) indicate that electronically these clay minerals are practically indistinguishable. In other words, this result suggests that stacking faults that lead to polytypism do not produce significant changes in the electronic properties of kaolins. However, there are very subtle changes on the DOS from one polytype to another that arise from their structural differences.

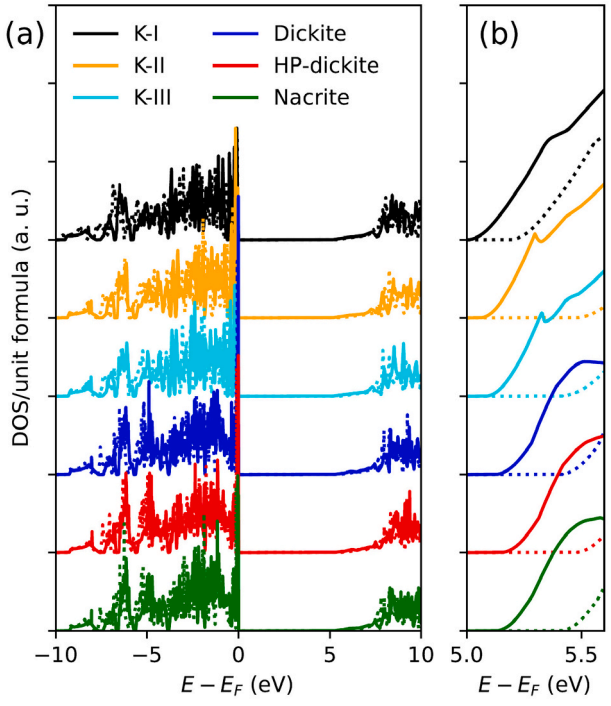

Fig. 7. (a) Comparison of the DOS at 0 GPa (solid lines) and 8 GPa (dotted lines) obtained with the PBE approximation, and (b) zoomed detail at the CB minima. Energy axis refers to the Fermi energy E_F.

Table 2
E_g values (in eV) obtained from the DOS calculated with the PBE approximation for hydrostatic pressures of 0 and 8 GPa.

Polytype	Pressure (GPa)	
	0	8
K-I	5.03	5.22
K-II	5.09	5.52
K-III	5.11	5.45
Dickite	5.16	5.44
HP-dickite	5.17	5.52
Nacrite	5.15	5.42

As shown in previous work for K-I (Richard and Rendtorff, 2019), the VB is mainly composed of O-2p states. The lower levels of the VB (those ranging from −10 to −7.5 eV in the solid lines of Fig. 7a) are due to the basal oxygen atoms (those at the Si tetrahedral sheet), while the inner and interlayer oxygen atoms (more related to the Al octahedral sheet) play a main role on the sharp peak at the top of the VB (at 0 eV). Si-3p, Al-3p, and H-1s orbitals have also a contribution to the VB, which evidence the bonding of these atoms with the O atoms. In particular, the H atoms, contributes to the lower part of the VB (from −7.5 to −6 eV in Fig. 7a), a region of the DOS where the subtle changes between polytypes may be more evident. This is due to the weak chemical bonding of the H atoms in the structure, so their relative positions to the layer fluctuate more easily from one polytype to another, *i.e.*, the interlayer OH groups can be oriented more or less perpendicularly to the layer. In the supplementary material are provided figures of each optimized structure that help to visualize this detail. But, as said, this effect of the structural properties on the DOS is very minor.

In comparison to the DOS obtained in this work, various previous DFT investigations have shown that the presence of point defects such as impurities and vacancies can substantially modify the Kaol K-I total DOS (Nisar et al., 2011; Pietzsch et al., 2015; Fu and Yang, 2017; Zhao et al., 2020; Richard and Rendtorff, 2021), producing larger changes to the DOS than those observed between polytypes in Fig. 7a. Therefore, considering that kaolin samples can present many bulk point defects such as isomorphous substitutions of Fe^{III}, Mg^{II} and Ti^{IV} for Al^{III} in the octahedral sheet (Brigatti et al., 2006), the role of layer slippings and stacking faults on the DOS should be considered secondary to them. Experimentally, due to the considerable influence of the point defects on the electronic structure of these clay minerals, there is still a lack of a consistent measurement for E_g in the literature. In this sense, only in the work of Pietzsch et al. (2015) was reported an experimental estimation for E_g for kaolinite, using X-ray absorption spectroscopy measurements and the aid of first-principles calculations. There, it was suggested that the true bandgap for pristine kaolinite is between 6.2 and 8.2 eV, and intrinsic defects can decrease it by about 3.2 eV.

In regard to the effect of the applied pressure on the electronic structure, in Fig. 7a are also the DOS for $P = 8$ GPa (in dotted lines), which allow the comparison to those corresponding to 0 GPa. As can be seen, the effect of pressure on the DOS is weak for this range of values: the VB becomes slightly wider and E_g is slightly increased in comparison to those corresponding to the 0 GPa case. For the last, in Fig. 7b there is a detail of the CB minima for each polytype at both pressures, 0 and 8 GPa, for better visualization of the subtle band shifts. The numerical values of E_g at 8 GPa are also presented in Table 2. In general, for all polytypes, the increment on the forbidden bandgap is in the range 0.2–0.3 eV (∼5% of the initial E_g value). These results are in very good agreement with those reported by Fang et al. (2017) for the K-I structure using DFT calculations, and indicate that a similar electronic behavior for all kaolin group polytypes can be expected in the whole range of pressures considered in this study.

4. Conclusions

The structural and electronic properties under pressure were determined by DFT methods for six kaolin group polytypes, which include the three naturally occurring polytypes Kaol K-I, dickite, and nacrite, and also other three polytypes experimentally observed when pressure is applied (K-II, K-III, and HP-dickite). For these purposes, the PBE and WC approximations for the exchange and correlation energy were used, which allowed assessing the accuracy of the DFT methods.

This DFT study gathers for the first time the optimized structures and the DOS of the six considered polytypes under pressure (< 10 GPa). The obtained predictions in this work were permanently compared to the available data in the literature, both experimental and theoretical. The optimized structures for the idealized defect-free polytypes provide additional insights to the recent discussions about the polytypes' relative stabilities and may help as guidance in experimentally difficult systems such as those into the kaolin group.

The differences between the obtained $E(V)$ data for the different polytypes are consistent with the known occurrence of stacking disorder in kaolinite samples, and the bulk modulus predictions suggest that those polytypes observed at higher pressures are more compressible and presumably less resistant to fracture than those of ambient pressure.

No significant changes were observed in the DOS among the different polytypes at the same pressure, and all of them show an insulator character with forbidden bandgap energy slightly above 5 eV. Also, this bandgap is increased by about 5% when pressure is increased to 8 GPa. From the comparison to previous experimental and theoretical studies, it is deduced that layer slippings play a minor role in the electronic properties of kaolinites, secondary to the presence of point defects in the structure of these clay minerals.

CRediT authorship contribution statement

D. Richard: Conceptualization, Methodology, Investigation, Software, Visualization, Writing – original draft. **N.M. Rendtorff:** Conceptualization, Supervision, Writing – review & editing.

Declaration of Competing Interest

The authors declare that they have no known competing financial interests or personal relationships that could have appeared to influence the work reported in this paper.

Acknowledgments

This work has been supported by the Argentinian funding institutions Consejo Nacional de Investigaciones Científicas y Técnicas (CONICET), Agencia Nacional de Promoción Científica y Tecnológica (ANPCyT, PICT 2019-03570), and Universidad Nacional de La Plata (UNLP, X-904). Part of the results presented in this work have been obtained by using the facilities of the CCT-Rosario Computational Center, member of the High Performance Computing National System (SNCAD, MinCyT-Argentina). The authors are members of CONICET, Argentina.

Appendix A. Supplementary data

Supplementary data to this article can be found online at https://doi.org/10.1016/j.clay.2022.106444.

References

Andrini, L., Gauna, M.R., Conconi, M.S., Suarez, G., Requejo, F.G., Aglietti, E.F., Rendtorff, N.M., 2016. Extended and local structural description of a kaolinitic clay, its fired ceramics and intermediates: an XRD and XANES analysis. Appl. Clay Sci. 124–125, 39–45. https://doi.org/10.1016/j.clay.2016.01.049.

Balan, E., Calas, G., Bish, D.L., 2014. Kaolin-Group minerals: from hydrogen-bonded layers to environmental recorders. Elements 10, 183–188. https://doi.org/10.2113/gselements.10.3.183.

Bayuk, I.O., Ammerman, M., Chesnokov, E.M., 2007. Elastic moduli of anisotropic clay. Geophysics 72, D107–D117. https://doi.org/10.1190/1.2757624.

Benazzouz, B.K., Zaoui, A., 2012a. A nanoscale simulation study of the elastic behaviour in kaolinite clay under pressure. Mater. Chem. Phys. 132, 880–888. https://doi.org/10.1016/j.matchemphys.2011.12.028.

Benazzouz, B.K., Zaoui, A., 2012b. Phase diagram of kaolinite from Molecular Dynamics calculations. Physica B 407, 2462–2470. https://doi.org/10.1016/j.physb.2012.03.047.

Birch, F., 1947. Finite elastic strain of cubic crystals. Phys. Rev. 71, 809. https://doi.org/10.1103/PhysRev.71.809.

Bish, D.L., 1993. Rietveld refinement of the kaolinite structure at 1.5 K. Clay Clay Miner. 41, 738–744. https://doi.org/10.1346/CCMN.1993.0410613.

Brigatti, M.F., Galan, E., Theng, B.K.G., 2006. Structures and mineralogy of clay minerals. Dev. Clay Sci. 1, 19–86. https://doi.org/10.1016/S1572-4352(05)01002-0.

Cuadros, J., Vega, R., Toscano, A., Arroyo, X., 2014. Kaolinite transformation into dickite during burial diagenesis. Am. Mineral. 99, 681–695. https://doi.org/10.2138/am.2014.4614.

Dal Corso, A., 2014. Pseudopotentials periodic table: from H to Pu. Comput. Mater. Sci. 95, 337. https://doi.org/10.1016/j.commatsci.2014.07.043.

De Ligny, D., Navrotsky, A., 1999. Energetics of kaolin polymorphs. Am. Mineral. 84, 506–516. https://doi.org/10.2138/am-1999-0404.

Dera, P., Prewitt, C.T., Japel, S., Bish, D.L., Johnston, C.T., 2003. Pressure-controlled polytypism in hydrous layered materials. Am. Mineral. 88, 1428–1435. https://doi.org/10.2138/am-2003-1006.

Detellier, Ch., 2018. Functional Kaolinite. Chem. Rec. 18, 868–877. https://doi.org/10.1002/tcr.201700072.

Fang, Z.J., Zhai, X.S., Li, Z.L., Pan, R.J., Mo, M., 2017. Pressure dependence of the electronic structure in kaolinite: a first-principles study. Mod. Phys. Lett. B 31, 1750194. https://doi.org/10.1142/S0217984917501949.

Fialips, C.I., Majzlan, J., Beaufort, D., Navrotsky, A., 2003. New thermochemical evidence on the stability of dickite vs. Kaolinite. Am. Mineral. 88, 837–845. https://doi.org/10.2138/am-2003-5-612.

Fossum, J.O., 2012. Flow of clays. Eur. Phys. J. Special Topics 204 (1), 41–56. https://doi.org/10.1140/epjst/e2012-01551-1.

Fu, L., Yang, H., 2017. Structure and electronic properties of transition metal doped kaolinite nanoclay. Nanoscale Res. Lett. 12, 411. https://doi.org/10.1186/s11671-017-2188-4.

Giannozzi, P., Andreussi, O., Brumme, T., Bunau, O., Buongiorno Nardelli, M., Calandra, M., Car, R., Cavazzoni, C., Ceresoli, D., Cococcioni, M., Colonna, N., Carnimeo, I., Dal Corso, A., De Gironcoli, S., Delugas, P., DiStasio Jr., R.A., Ferretti, A., Floris, A., Fratesi, G., Fugallo, G., Gebauer, R., Gerstmann, U., Giustino, F., Gorni, T., Jia, J., Kawamura, M., Ko, H.Y., Kokalj, A., Kucukbenli, E., Lazzeri, M., Marsili, M., Marzari, N., Mauri, N., Nguyen, N.L., Nguyen, H.V., Otero-de-la-Roza, A., Paulatto, L., Poncé, S., Rocca, D., Sabatini, R., Santra, B., Schlipf, M., Seitsonen, A.P., Smogunov, A., Timrov, I., Thonhauser, T., Umari, P., Vast, N., Wu, W., Baroni, S., 2017. Advanced capabilities for materials modelling with Quantum ESPRESSO. J. Phys. Condens. Matter 29, 465901. https://doi.org/10.1088/1361-648X/aa8f79.

Grimme, S., 2006. Semiempirical GGA-type density functional constructed with a long-range dispersion correction. J. Comput. Chem. 27, 1787. https://doi.org/10.1002/jcc.20495.

Guggenheim, S., Adams, J.M., Bergaya, F., Brigatti, M.F., Drits, V.A., Formoso, M.L.L., Galán, E., Kogure, T., Stanjek, H., Stucki, J.W., 2009. Nomenclature for stacking in phyllosilicates: report of the Associoation Internationale Pour l'Etude des Argiles (AIPEA) Nomenclature Comittee for 2008. Clay Clay Miner. 57, 134–135. https://doi.org/10.1346/CCMN.2009.0570112.

Haas, P., Tran, F., Blaha, P., 2009. Calculation of the lattice constant of solids with semilocal functionals. Phys. Rev. B 79, 085104. https://doi.org/10.1103/PhysRevB.79.085104.

Hwang, H., Seoung, D., Lee, Y., Liu, Z., Liermann, H.P., Cynn, H., Vogt, T., Kao, C.C., Mao, H.K., 2017. A role for subducted super-hydrated kaolinite in Earth's deep water cycle. Nat. Geosci. 10, 947–953. https://doi.org/10.1038/s41561-017-0008-1.

Hwang, H., Choi, J., Liu, Z., Kim, D.Y., He, Y., Celestian, A.J., Vogt, T., Lee, Y., 2020. Pressure-induced hydration and formation of bilayer ice in nacrite, a kaolin-group clay. ACS Earth Space Chem. 4, 183–188. https://doi.org/10.1021/acsearthspacechem.9b00255.

Johnston, C.T., Wang, S.L., Bish, D.L., Dera, P., Agnew, S.F., Kenney, J.W., 2002. Novel pressure-induced phase transformations in hydrous layered materials. Geophys. Res. Lett. 29, 17-1-17-4. https://doi.org/10.1029/2002GL015402.

Kiseleva, I.A., Orogodova, L.P., Krupskaya, V.V., Melchakova, L.V., Vigasina, M.F., Luse, I., 2011. Thermodynamics of the kaolinite-group minerals. Geochem. Int. 49, 793–801. https://doi.org/10.1134/S001670291106005X.

Kogure, T., Inoue, A., 2005. Stacking defects and long-period polytypes in kaolin minerals from a hydrothermal deposit. Eur. J. Mineral. 17, 465–473. https://doi.org/10.1127/0935-1221/2005/0017-0465.

Kogure, T., Elzea-Kogel, J., Johnston, C.T., Bish, D.L., 2010. Stacking disorder in a sedimentary kaolinite. Clay Clay Miner. 58, 62–71. https://doi.org/10.1346/ccmn.2010.0580106.

Manning, D.C., 2003. Experimental studies of clay mineral occurrence. In: Worden, R.H., Morad, S. (Eds.), Clay Mineral Cements in Sandstones. Int. Assoc. Sedimentol. Spec. Publ., Wiley. https://doi.org/10.1002/9781444304336.ch9.

Mercier, P.H.J., Le Page, Y., 2008. Kaolin polytypes revisited ab initio. Acta Cryst B64, 131–143. https://doi.org/10.1107/S0108768108001924.

Mercier, P.H.J., Le Page, Y., 2009. Ab initio exploration of layer slipping transformations in kaolinite up to 60 GPa. Mater. Sci. Technol. 25, 437–442. https://doi.org/10.1179/174328408X371958.

Mercier, P.H.J., Le Page, Y., 2011. Rational ab initio modeling for low energy hydrogen-bonded phyllosilicate polytypes. Eur. J. Mineral. 23, 401–407. https://doi.org/10.1127/0935-1221/2011/0023-2092.

Mercier, P.H.J., Le Page, Y., Desgrenier, S., 2010. Kaolin polytypes revisited ab initio at 10 GPa. Am. Mineral. 95, 1117–1120. https://doi.org/10.2138/am.2010.3503.

Mikowski, A., Soares, P., Wypych, F., Gardolinski, J.E.F.C., Lepienski, C.M., 2007. Mechanical properties of kaolinite 'macro-crystals'. Philos. Mag. 87 (29), 4445–4459. https://doi.org/10.1080/14786430701550394.

Momma, K., Izumi, F., 2011. VESTA 3 for three-dimensional visualization of crystal, volumetric and morphology data. J. Appl. Crystallogr. 44, 1272–1276. https://doi.org/10.1107/S0021889811038970.

Mori-Sánchez, P., Cohen, A.J., Yang, W., 2008. Localization and delocalization errors in Density Functional Theory and implications for band-gap prediction. Phys. Rev. Lett. 100, 146401 https://doi.org/10.1103/PhysRevLett.100.146401.

Murray, H.H., 1988. Kaolin minerals: their genesis and occurrences. Rev. Minerarol. 19 https://doi.org/10.1515/9781501508998.

Newnham, R., 1961. A refinement of the dickite structure and some remarks on polymorphism in kaolin minerals. Mineral. Mag. J. Mineral. Soc. 32 (252), 683–704. https://doi.org/10.1180/minmag.1961.032.252.03.

Nisar, J., Århammar, C., Jämstorp, E., Ahuja, R., 2011. Optical gap and native point defects in kaolinite studied by the GGA-PBE, HSE functional, and GW approaches. Phys. Rev. B 84, 075120. https://doi.org/10.1103/PhysRevB.84.075120.

Pavese, A., 2005. About the relations between finite strain in non-cubic crystals and the related phenomenological P-V Equation of State. Phys. Chem. Miner. 2, 269–276. https://doi.org/10.1007/s00269-005-0465-8.

Perdew, J.P., Burke, K., Ernzerhof, M., 1996. Generalized gradient approximation made simple. Phys. Rev. Lett. 77 https://doi.org/10.1103/PhysRevLett.77.3865, 3865; and 1997 PRL 78, 1396 (E).

Pietzsch, A., Nisar, J., Jämstorp, E., Gråsjö, J., Århammar, C., Ahuja, R., Rubensson, J.E., 2015. Kaolinite: defect defined material properties - a soft X-ray and first principles study of the band gap. J. Electron Spectros. Relat. Phenomena 202, 11. https://doi.org/10.1016/j.elspec.2015.02.003.

Prandini, G., Marrazzo, A., Castelli, I.E., Mounet, N., Marzari, N., 2018. Precision and efficiency in solid-state pseudopotential calculations. NPJ Comput. Mater. 4, 72. https://doi.org/10.1038/s41524-018-0127-2.

Richard, D., Rendtorff, N.M., 2019. First principles study of structural properties and electric field gradients in kaolinite. Appl. Clay Sci. 169, 67. https://doi.org/10.1016/j.clay.2018.12.013.

Richard, D., Rendtorff, N.M., 2021. Local environments in iron-bearing clay minerals by DFT approaches: the case of structural Fe in kaolinite. Appl. Clay Sci. 213, 106251 https://doi.org/10.1016/j.clay.2021.106251.

Richard, D., Errico, L.A., Rentería, M., 2016. Structural properties and the pressure-induced C/a phase transition of lanthanide sesquioxides from DFT and DFT+U calculations. J. Alloys Compd. 664, 580–589. https://doi.org/10.1016/j.jallcom.2015.12.236.

Richard, D., Martínez, J.M., Mizrahi, M., Andrini, L., Rendtorff, N.M., 2022. Assessment of structural order indices in Kaolinites: a multi-technique study including EXAFS. J. Electron Spectrosc. Relat. Phenom. 254, 147128 https://doi.org/10.1016/j.elspec.2021.147128.

Sakharov, B.A., Drits, V.A., McCarty, D.K., Walker, G.M., 2016. Modeling powder X-ray diffraction patterns of the Clay Minerals Society kaolinite standards: KGa-1, KGa-1b, and Kga-2. Clay Clay Miner. 64, 314–333. https://doi.org/10.1346/CCMN.2016.0640307.

Sato, H., Ono, K., Johnston, L.T., Yamagishi, A., 2004. First-principle study of polytype structures of 1:1 dioctahedral phyllosilicates. Am. Mineral. 89, 1581–1585. https://doi.org/10.2138/am-2004-11-1201.

Sato, H., Ono, K., Johnston, L.T., Yamagishi, A., 2005. First-principles studies on the elastic constants of a 1:1 layered kaolinite mineral. Am. Mineral. 90, 1824–1826. https://doi.org/10.2138/am.2005.1832.

Schroeder, P.A., Erickson, G., 2014. Kaolin: from ancient porcelains to nanocomposites. Elements 10, 177–182. https://doi.org/10.2113/gselements.10.3.177.

Seredin, V.V., Rastegaev, A.V., Galkin, V.I., Isaeva, G.A., Yu Parshina, T., 2018. Changes of energy potential on clay particle surfaces at high pressures. Appl. Clay Sci. 155, 8–14. https://doi.org/10.1016/j.clay.2017.12.042.

Shafei, L., Adhikari, P., Ching, W.Y., 2021. DFT study of electronic structure and optical properties of kaolinite, muscovite, and montmorillonite. Crystals 11, 618. https://doi.org/10.3390/cryst11060618.

Soto, J.I., Hudec, M.R., Mondol, N.H., Heidari, M., 2021. Shale transformations and physical properties-implications for seismic expression of mobile shales. Earth-Sci. Rev. 220, 103746 https://doi.org/10.1016/j.earscirev.2021.103746.

Teixeira, C.E., Brandão, P.R.G., Nunes, R.W., 2017. Methodological reconstruction of dioctahedral 1:1 phyllosilicate polytypes. Appl. Clay Sci. 146, 201–205. https://doi.org/10.1016/j.clay.2017.06.001.

Tran, F., Laskowski, R., Blaha, P., Schwarz, K., 2007. Performance on molecules, surfaces, and solids of the Wu-Cohen GGA exchange-correlation energy functional. Phys. Rev. B 75, 115131. https://doi.org/10.1103/PhysRevB.75.115131.

Tunega, D., Bučko, T., Zaoui, A., 2012. Assessment of ten DFT methods in predicting structures of sheet silicates: importance of dispersion corrections. J. Chem. Phys. 137, 114105 https://doi.org/10.1063/1.4752196.

Vanorio, T., Prasad, M., Nur, A., 2003. Elastic properties of dry clay mineral aggregates, suspensions and sandstones. Geophys. J. Int. 155, 319–326. https://doi.org/10.1046/j.1365-246X.2003.02046.x.

Wang, Z.Z., Wang, H., Cates, M.E., 2001. Effective elastic properties of solid clays. Geophysics 66, 428–440. https://doi.org/10.1190/1.1444934.

Weck, P.F., Kim, E., Jové-Colón, C.F., 2015. Relationship between crystal structure and thermo-mechanical properties of kaolinite clay: beyond standard density functional theory. Dalton Trans. 44, 12550. https://doi.org/10.1039/c5dt00590f.

Welch, M.D., Crichton, W., 2010. Pressure-induced transformations in kaolinite. Am. Mineral. 95, 651–654. https://doi.org/10.2138/am.2010.3408.

Welch, M.D., Montgomery, W., Balan, E., Lerch, P., 2012. Insights into the high-pressure behavior of kaolinite from infrared spectroscopy and quantum-mechanical calculations. Phys. Chem. Miner. 39, 143–151. https://doi.org/10.1007/s00269-011-0469-5.

Wu, Z., Cohen, R.E., 2006. More accurate generalized gradient approximation for solids. Phys. Rev. B 73, 235116. https://doi.org/10.1103/PhysRevB.73.235116.

Yang, H., Tong, D., Dong, Y., Ren, L., Fang, K., Zhou, C., Yu, W., 2020. Kaolinite: a natural and stable catalyst for depolymerization of cellulose to reducing sugars in water. Appl. Clay Sci. 188, 105512 https://doi.org/10.1016/j.clay.2020.105512.

Zhang, L.L., Zheng, Y.Y., Wei, P.C., Diao, Q.F., Yin, Z.Y., 2021. Nanoscale mechanical behavior of kaolinite under uniaxial strain conditions. Appl. Clay Sci. 201, 105961 https://doi.org/10.1016/j.clay.2020.105961.

Zhao, J., Qin, X., Wang, J., He, M., 2020. Effect of Mg(II) and Na(I) doping on the electronic structure and mechanical properties of kaolinite. Minerals 10, 368. https://doi.org/10.3390/min10040368.

Zhao, B., Liu, L., Cheng, H., 2021. Rational design of kaolinite-based photocatalytic materials for environment decontamination. Appl. Clay Sci. 208, 106098 https://doi.org/10.1016/j.clay.2021.106098.

Zhukhlistov, A.P., 2008. Crystal structure of nacrite from the electron diffraction data. Crystallogr. Rep. 53, 76–82. https://doi.org/10.1134/S1063774508010094.